Constructing Spin Density Vector Twists With Spin Density Singularity

Xiaoyan Pang, *Member, IEEE*, Han Zhang, Mingze Hu, and Xinying Zhao

***Abstract*—In this article, we propose a non-orbital angular momentum (OAM) method for constructing the spiral twists of spin density (SD) vectors in three-dimensional (3D) optical fields. This is realized by generating strings of SD singularities in a longitudinal plane of a strongly focused HG10 mode beam with circular polarization. We demonstrate that in this plane, the SD singularities manifest themselves as the Gouy phase difference. Through observing the Gouy phase difference, the strings of the SD singularities and their topological reactions are examined. It is found that the spiral twists of SD vectors are constructed in the two-dimensional (2D) space between two strings and their twisting behaviors can be adjusted by the topological reactions of the strings. This finding shows that the spiral twists can be formed in a 2D space rather than the 1D space in previous studies, which provides a more flexible way to utilize this rotational degree of freedom. Our result also clarifies that although the spiral twists of SD vectors can be a result of spin-orbital angular momentum interaction, the OAM is not a necessary condition for the generation of these twists. Our theoretical proposal for structuring SD vectors may have applications in 3D optical manipulation.**

***Index Terms*—Spin density, optical singularity, orbital angular momentum, spin angular momentum, Gouy phase.**

I. Introduction

EXPLORING new freedoms of optical fields and controlling them is one of the main aims in optical studies, ranging from utilizing intensity in lighting, applying phase/polarization/coherence (the nowadays well-known freedoms) in holography, liquid-crystal displays, optical coherence tomography, etc [1]–[3], to employing optical momenta, including linear momentum and angular momentum in optical manipulation [4]–[7]. New freedom always opens up novel capabilities of light. Spin angular momentum (SAM) density, also called spin density, is usually a scalar quantity in two-dimensional (2D) fields to express the density of the SAM with direction, while in a three-dimensional (3D) vector field, it becomes a vector, and the spin density (SD) vector supplies a new freedom in structuring 3D vector fields [8]–[12]. Studies on SD vectors have become a field with rapidly growing interest [13]–[26], and the new features have been found in 3D nano-optics, such as their effect in controlling light–matter interaction on the level of individual atoms [27], in the emission directivity of a dipole-like nano-particle [28]. The transverse component of the SD vector has been demonstrated to have a close connection with geometrical spin Hall effect of light [29]–[36], and when the SD vectors are purely transverse, the 'photonic wheel' phenomenon occurs, which has promising applications in on-chip and inter-chip optical circuitry and optical quantum computing [13], [14], [17], [24]. Especially, it is interesting to find that the SD vectors can rotate along the propagation direction, i.e. the spiral twists of SD vectors can be constructed in 3D space [19]. Since the spiral twists of SD vectors can provide a new rotational degree of freedom in 3D optical manipulation, a number of 3D vector fields have been proposed for generating the spiral twists of SD vectors [20]–[22], [25], [26]. However, there may exist two problems in these reported researches. In all these fields, the orbital angular momentum (OAM) is used for generating the twists, and it is also found that the spiral twist of SD vectors is a result of the spin-orbital interactions (SOIs) [19]–[21], [37]. So, one problem is: there seems a misunderstanding that the OAM is a necessary condition for the generation of the spiral twist of SD vectors. The other problem is the tiny space of the spiral twists, i.e., the spiral twists are generated along one optical axis in all previous researches. This means that the spiral twists only exist in a very narrow region, i.e., in the one dimensional (1D) space, which may limit the application of this rotational degree of freedom. Here we will propose a new way to construct these spiral twists and show that the OAM can be absent from the generation of these spiral twists, and these twists can occur in a wide region, i.e, in a 2D space.

When 3D optical fields are observed from the topological view, there will exhibit distinctive scenes. Around a C point the long axes of the polarization ellipses compose Möbius strips [38]–[40], a fully structured optical field can exhibit topological 3D skyrmionic hopfion [41], and the phase/polarization singular lines may be knotted in different shapes [12], [42], [43]. Although the topological behaviors of these singularities obey the sign rule [44], they will do some 'disordered' reactions locally because of the Berry's paradox [45]–[47]. Very recently, it is found some new optical singularities hidden in 3D vector fields and unique to these fields [48]. They are SD singularities, including SD phase singularity and SD vector singularity, which

Manuscript received December 13, 2021; revised March 21, 2022; accepted April 2, 2022. Date of publication April 5, 2022; date of current version April 26, 2022. This work was supported in part by the National Natural Science Foundation of China under Grants 11974281 and 12104283 and in part by Natural Science Basic Research Plan in Shaanxi Province of China under Grant 2020JM-116. *(Corresponding author: Xiaoyan Pang; Xinying Zhao.)*

Xiaoyan Pang, Han Zhang, and Mingze Hu are with the School of Electronics and Information, Northwestern Polytechnical University, Xi'an 710072, China (e-mail: xypang@nwpu.edu.cn; hanzhang@mail.nwpu.edu.cn; 2021262254@mail.nwpu.edu.cn).

Xinying Zhao is with the School of Physics and Information Technology, Shaanxi Normal University, Xi'an 710061, China (e-mail: zhaoxinying@snnu.edu.cn).

Digital Object Identifier 10.1109/JPHOT.2022.3165090

characterize the phase distribution and the vector structure of the 3D vector fields respectively. The SD singularities also follow the topological rules of singular optics and have a close connection with the conventional optical singularities [48]. The complexity of the SD singularities usually causes them hard to be observed. Here we will show that under certain circumstances, the SD singularities can express themselves through another physical quantity, which is more convenient to examine. More importantly, it will be seen in this article that the SD singularities are the essential ingredient for constructing the spiral twists of SD vectors.

II. Theory

A. SD Vector and SD Singularity

In general, an electromagnetic field is 3D, and a fully polarized electric field can be expressed as (the time-dependent is suppressed)

$$\mathbf{E} = \begin{pmatrix} e_x \\ e_y \\ e_z \end{pmatrix} = \begin{pmatrix} |e_x|\, e^{\mathrm{i}\phi_x} \\ |e_y|\, e^{\mathrm{i}\phi_y} \\ |e_z|\, e^{\mathrm{i}\phi_z} \end{pmatrix}, \tag{1}$$

where ϕ_i $(i = x, y, z)$ denotes the phase of the Cartesian field component e_i. At a point of this 3D electric field, the polarization ellipse can lie in any plane in the 3D space. The SD vector, $\mathbf{s}_E$ as a quantity describing the 3D polarization state, is given by [9], [14], [19]:

$$\begin{aligned} \mathbf{s}_E &= \frac{\epsilon_0}{4\omega}\mathrm{Im}(\mathbf{E}^* \times \mathbf{E}) = \begin{pmatrix} s_E^{(x)} \\ s_E^{(y)} \\ s_E^{(z)} \end{pmatrix} \\ &= \frac{\epsilon_0}{2\omega}\begin{pmatrix} |e_y||e_z|\sin\phi_{zy} \\ |e_x||e_z|\sin\phi_{xz} \\ |e_x||e_y|\sin\phi_{yx} \end{pmatrix}, \end{aligned} \tag{2}$$

where ω denotes the angular frequency and ϵ_0 is the permittivity of free space. Im represents the imaginary part and $*$ means the complex conjugate. $\phi_{ij} = \phi_i - \phi_j$, $(i, j = x, y, z)$ is the phase difference between two components. In many optical fields, such as the fields in a high numerical aperture (NA) system, the phase difference ϕ_{ij} is actually the Gouy phase difference δ_{ij}, i.e., $\phi_{ij} = \delta_{ij} = \delta_i - \delta_j$ [19], [49]–[51]. Here δ_i is the Gouy phase of the field component e_i, which is defined as the phase difference between the actual optical field and the ideal field (without diffraction) [1], i.e.

$$\delta_i = \arg[e_i] - kR, (i = x, y, z) \tag{3}$$

where arg means the phase/argument of the field component, $k = 2\pi/\lambda$ is the wave number and R is the distance between the observed point and the focus.

SD singularities are characteristic singularities of the 3D vector field [48], including the SD phase singularity and the SD vector singularity. A SD phase singularity occurs when the complex SD field, $s_E^{(ij)}$ $(i, j = x, y, z; i \neq j)$ expressed as

$$\begin{aligned} s_E^{(ij)} &= s_E^{(i)} + \mathrm{i}s_E^{(j)}, \\ &(i, j = x, y, z; \tilde{}\tilde{} i \neq j) \end{aligned} \tag{4}$$

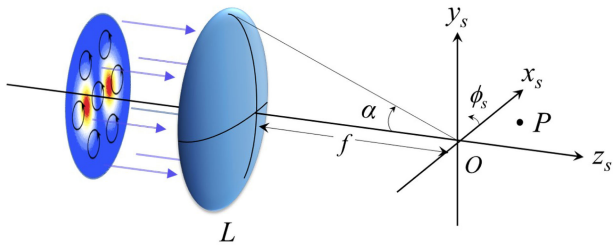

Fig. 1. Schematic illustration of a high NA system.

has null intensity. That is $|s_E^{(i)}| = |s_E^{(j)}| = 0$, thus the phase of $s_E^{(ij)}$ is undefined. The SD vector singularity means that the direction of the SD vector is undefined, which happens if the (total) SD is zero. So a SD vector singularity is formed at the point with $|s_E^{(x)}| = |s_E^{(y)}| = |s_E^{(z)}| = 0$. The definitions of these two types of SD singularities also indicate that when two kinds of SD phase singularities, for example the phase singularities of $s_E^{(xy)}$ and $s_E^{(yz)}$ coincide at one point, this point must be a SD vector singularity.

B. 3D Optical Field in a High NA System

In this section a non-vortex beam with circular polarization is considered as the incident beam of a high NA system for forming strings of SD singularities in the focal region.

First, this incident beam is a beam of the HG10 mode which is left-handed circularly polarized (LCP), and at the beam waist plane it can be expressed as [52]:

$$\mathbf{E}^{(in)}(x, y) = \begin{pmatrix} e_x^{(in)} \\ e_y^{(in)} \end{pmatrix} = xe^{-(x^2+y^2)/w_0^2}\begin{pmatrix} 1 \\ \mathrm{i} \end{pmatrix}, \tag{5}$$

where w_0 is the waist size. (5) also can be written in polar coordinates by using $x = r\cos\phi, y = r\sin\phi$. Note this incident beam only carries SAM but not OAM.

Second, consider a high NA system with the focal length f and a semi-aperture angle α (see Fig. 1). The focus of this system is set at the origin of the coordinate system. Assume that the HG10 beam expressed by (5) is incident upon this focusing system with its the waist plane coincident with the entrance plane of the system. Then the 3D electric field at point (ρ_s, ϕ_s, z_s) in the focal region can be derived through applying the Richards-Wolf vectorial diffraction theory [53], as

$$\mathbf{E}^{(f)}(\rho_s, \phi_s, z_s) = \hat{x}e_x^{(f)} + \hat{y}e_y^{(f)} + \hat{z}e_z^{(f)}, \tag{6}$$

and

$$e_x^{(f)}(\rho_s, \phi_s, z_s) = -\mathrm{i}k\int_0^\alpha P(\theta)I_x(\theta; \rho_s, \phi_s)e^{\mathrm{i}kz_s\cos\theta}\mathrm{d}\theta, \tag{7}$$

$$e_y^{(f)}(\rho_s, \phi_s, z_s) = -\mathrm{i}k\int_0^\alpha P(\theta)I_y(\theta; \rho_s, \phi_s)e^{\mathrm{i}kz_s\cos\theta}\mathrm{d}\theta, \tag{8}$$

$$e_z^{(f)}(\rho_s, \phi_s, z_s) = -\mathrm{i}k\int_0^\alpha P(\theta)I_z(\theta; \rho_s, \phi_s)e^{\mathrm{i}kz_s\cos\theta}\mathrm{d}\theta, \tag{9}$$

where

$$P(\theta) = \sqrt{\cos\theta}(f\sin\theta)^2 e^{-(f\sin\theta)^2/w_0^2}, \tag{10}$$

$$\begin{aligned} &I_x(\theta;\rho_s,\phi_s) \\ &= \frac{1}{4}\left[(1-\cos\theta)\sin\phi_s + \mathrm{i}\,(3\cos\theta+1)\cos\phi_s\right] \\ &\quad J_1\left(k\rho_s\sin\theta\right) \\ &\quad + \mathrm{i}\frac{1}{4}\left(1-\cos\theta\right)e^{\mathrm{i}3\phi_s}J_3\left(k\rho_s\sin\theta\right), \end{aligned} \tag{11}$$

$$\begin{aligned} &I_y(\theta;\rho_s,\phi_s) \\ &= \frac{1}{4}\left[\mathrm{i}\,(\cos\theta-1)\sin\phi_s - (3+\cos\theta)\cos\phi_s\right] \\ &\quad J_1\left(k\rho_s\sin\theta\right) \\ &\quad + \frac{1}{4}\left(1-\cos\theta\right)e^{\mathrm{i}3\phi_s}J_3\left(k\rho_s\sin\theta\right), \end{aligned} \tag{12}$$

$$\begin{aligned} &I_z(\theta;\rho_s,\phi_s) \\ &= \frac{1}{2}\sin\theta\left[-J_0\left(k\rho_s\sin\theta\right) + e^{\mathrm{i}2\phi_s}J_2\left(k\rho_s\sin\theta\right)\right]. \end{aligned} \tag{13}$$

In the equations above $J_n(x)$ represents the Bessel function of first kind with order n. Since the incident field is LCP, it is convenient to re-write the transverse component of the focused field into a sum of orthogonal circularly polarized components, i.e., a LCP component and a right circularly polarized (RCP) component. Thus (6) can be written as:

$$\mathbf{E}^{(f)}(\rho_s,\phi_s,z_s) = \begin{bmatrix}1\\ \mathrm{i}\\ 0\end{bmatrix} e^{(f)}_{\mathrm{LCP}} + \begin{bmatrix}1\\ -\mathrm{i}\\ 0\end{bmatrix} e^{(f)}_{\mathrm{RCP}} + \begin{bmatrix}0\\ 0\\ 1\end{bmatrix} e^{(f)}_z, \tag{14}$$

with

$$\begin{aligned} &e^{(f)}_{\mathrm{LCP}}(\rho_s,z_s,\phi_s) \\ &= \frac{k}{2}\int_0^{\alpha} P(\theta)\left(1+\cos\theta\right)\cos\phi_s J_1\left(k\rho_s\sin\theta\right)e^{\mathrm{i}kz_s\cos\theta}\mathrm{d}\theta, \end{aligned} \tag{15}$$

$$\begin{aligned} &e^{(f)}_{\mathrm{RCP}}(\rho_s,z_s,\phi_s) = \frac{k}{4}\int_0^{\alpha} P(\theta)\left(\cos\theta-1\right) \\ &\times\left[e^{i\phi_s}J_1\left(k\rho_s\sin\theta\right) - e^{i3\phi_s}J_3\left(k\rho_s\sin\theta\right)\right]e^{\mathrm{i}kz_s\cos\theta}\mathrm{d}\theta. \end{aligned} \tag{16}$$

The analyses and the results in the following are mainly based on the expressions of this 3D field.

In this section, we introduce a method to generate a 3D vector field by focusing a HG10 beam without OAM in a high NA system. As it will be seen in the following, by present method the spiral twists of the SD vectors can be constructed and their behaviors are closely related to the SD singularities.

III. Results and Discussions

From (16), we can find that when $\phi_s = \pm 90^\circ$, $e^{(f)}_{LCP} = 0$, which means that only $e^{(f)}_{RCP}$ and $e^{(f)}_z$ components left in the y_sOz_s-plane. As we will see soon, because of this special property very interesting phenomena can be observed in this plane.

A. SD Singularity and Gouy Phase

Here we will discuss the SD singularity in the y_sOz_s-plane. By putting $\phi_s = \pm 90^\circ$ into Eqs. (7–13), we can get $e^{(f)}_x = \mathrm{i}e^{(f)}_y$. This implies:

$$\left|e^{(f)}_x\right| = \left|e^{(f)}_y\right|, \tag{17}$$

$$\delta^{(f)}_{yx} = \delta^{(f)}_y - \delta^{(f)}_x = \phi^{(f)}_y - \phi^{(f)}_x = -\pi/2, \tag{18}$$

here $\delta^{(f)}_{ij}$ is the Gouy phase difference between the $e^{(f)}_i$ and the $e^{(f)}_j$ $(i,j = x,y,z)$ components of the focused field. Also since $\delta^{(f)}_{zy} = \delta^{(f)}_z - \delta^{(f)}_y = -(-\delta^{(f)}_{xz} + \delta^{(f)}_{yx}) = -\delta^{(f)}_{xz} + \pi/2$, the SD vector in the y_sOz_s-plane becomes

$$\mathbf{s}_E = \begin{pmatrix} s^{(x)}_E \\ s^{(y)}_E \\ s^{(z)}_E \end{pmatrix} = \frac{\epsilon_0}{2\omega}\begin{pmatrix} \left|e^{(f)}_x\right|\left|e^{(f)}_z\right|\cos\delta^{(f)}_{xz} \\ \left|e^{(f)}_x\right|\left|e^{(f)}_z\right|\sin\delta^{(f)}_{xz} \\ -\left|e^{(f)}_x\right|^2 \end{pmatrix}. \tag{19}$$

From the definition of the SD singularity and (19), we can get that in the y_sOz_s-plane the SD phase singularity will be found at the point with $|e^{(f)}_z| = 0$, and the SD vector singularity will be seen at the point with $|e^{(f)}_x| = 0$ (note this point also is a SD phase singularity). Thus, we can conclude that if

$$|e^{(f)}_x||e^{(f)}_z| = 0, \tag{20}$$

the SD singularity will happen. Let us recall the meaning of the Gouy phase difference $\delta^{(f)}_{xz}$. $\delta^{(f)}_{xz}$ is exactly the phase of the expression $e^{(f)}_x e^{*(f)}_z$, i.e.

$$\delta^{(f)}_{xz} = \arg\left[e^{(f)}_x e^{*(f)}_z\right], \tag{21}$$

which means that if (20) is satisfied, the Gouy phase difference $\delta^{(f)}_{xz}$ is undefined, i.e. the singularity of $\delta^{(f)}_{xz}$ will happen. Thus we can get an conclusion: *In the y_sOz_s-plane the SD singularities can manifest themselves as the singularities of the Gouy phase difference $\delta^{(f)}_{xz}$*. Therefore, the SD singularity can be analyzed through a more convenient way i.e., observing the Gouy phase difference $\delta^{(f)}_{xz}$, the more direct physical quantity. This also can be seen clearly in Fig. 2.

In Fig. 2(a), the SD vectors of the focused field for $\phi_s = \pm 90^\circ$ (in the y_sOz_s-plane, with $2\lambda < z_s < 6\lambda$ and $-2\lambda < y_s < 2\lambda$) are drawn, and their projection on the y_sOz_s-plane is displayed in Fig. 2(b), where the arrows in small scale (such as the arrows near points (3,0) and (5,0)) indicate that the $s^{(x)}_E$ is the leading component there. The corresponding Gouy phase difference $\delta^{(f)}_{xz}$ is drawn in Fig. 2(c), where $\delta^{(f)}_{xz}$ is set between $-\pi$ to $+\pi$. In all plots $\alpha = 60^\circ$, $f/w_0 = 2$. In Fig. 2(c), the intersections of different contours are the singularities of $\delta^{(f)}_{xz}$, which also represent the SD singularities. It is quite clear that the SD singularities are easier to identify in the phase-type illustration, for example the singular points 'A' and 'B' are the intersections

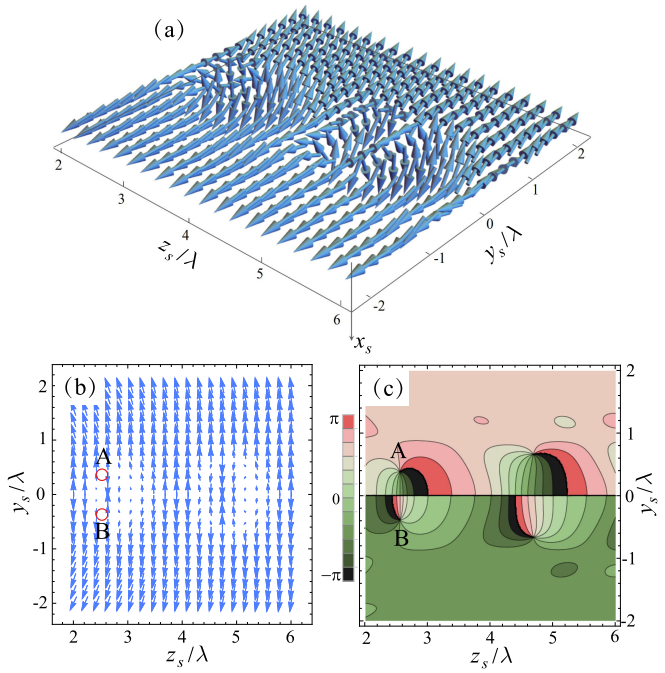

Fig. 2. Distribution of the SD vectors in the y_sOz_s-plane of the focused field. (a) The SD vectors in the 3D space, (b) the projection of the SD vectors on the 2D space, the y_sOz_s plane, (c) the Gouy phase difference $\delta_{xz}^{(f)}$ in the y_sOz_s-plane, where the intersections of different contours indicate the singularities of the Gouy phase difference, and also the SD singularities. Here $\alpha = 60°$.

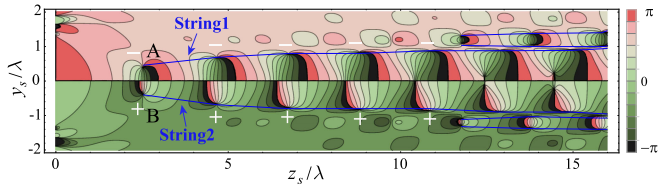

Fig. 3. SD singularity strings in the y_sOz_s-plane for $\alpha = 60°$.

of contours in Fig. 2(c), while in Fig. 2(a) and (b) these two points need more SD vectors to identify their local topological structures. Therefore, from here on, the Gouy phase difference $\delta_{xz}^{(f)}$ is used to examine the behaviors of the SD singularities.

The Gouy phase difference $\delta_{xz}^{(f)}$ in the y_sOz_s-plane with a wide region is illustrated in Fig. 3, where the parameters are the same as in Fig. 2. It is interesting to see that there exist 'strings' of SD singularities in the y_sOz_s-plane (the singularities in the same string are connected by a blue curve in Fig. 3), and since the infinite propagation distance, these SD singularity strings are theoretically infinite in length. The strings appear in pair as the singularities do, and the topological charge for each SD singularity along the longer string in upper space ($y_s > 0$, labeled by 'String1') is -1 which is opposite to the charge of any singularity on the corresponding string in lower space ($y_s < 0$, labeled by 'String2'). The charges of the first five pairs of singularities along String1 and String2 are marked in white.

Here we will see that as the semi-aperture angle α changes, the SD singularity strings are 'plucked'. For $\alpha = 65°$ and $70°$, the distributions of the SD singularities are shown in Fig. 4. We can find that with the increase of α, more singularities 'crowd'

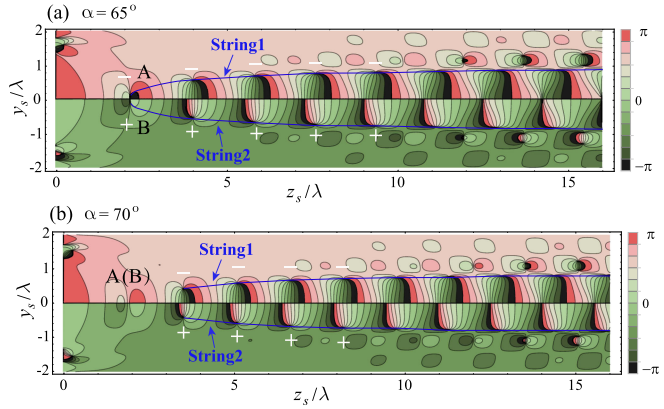

Fig. 4. SD singularity strings in the y_sOz_s-plane for (a)$\alpha = 65°$, (b)$\alpha = 70°$.

into the region near focus, in other words there are more SD singularities in the same region. For instance there exist 7 pairs of singularities along String1 and String2 in Fig. 3 for $\alpha = 60°$, while there are more than 8 pairs in Fig. 4(b) for $\alpha = 70°$. At the same time, as α increases (from 60° to 70°), the annihilation occurs topologically. The SD singularity A with charge -1 annihilates with point B with charge $+1$ (see Figs. 3 and 4). Such a topological event will continue to happen when α keeps increasing, which means that the pairs of the SD singularities along two long strings (String1 and String2) will annihilate one by one if α gets bigger and bigger. Additionally, when α becomes larger, one also can find that the positions of the SD singularity strings move slightly closer to the optical axis, for instance when $\alpha = 60°$ the second singularity in Sting1 is located at $y_s = 0.72\lambda$, while when $\alpha = 70°$ it is located at $y_s = 0.63\lambda$.

These phase structures around the SD singularities, as we will see in the following, can induce the twists of SD vectors, and the positions of the strings will decide the shapes of the twists.

B. SD Vector Twists

From (19), one can find that $s_E^{(z)}$ only depends on the absolute value of $e_x^{(f)}$, thus the longitudinal component of the SD vector always points to $-z_s$ direction in the y_sOz_s-plane (except the points with $|e_x^{(f)}| = 0$), while $s_E^{(y)}/s_E^{(x)} = \tan\delta_{xz}^{(f)}$ implies that the trajectory of the transverse component of the SD vector can be a circle. These two factors lead to a result: the twists of SD vectors can be constructed in the y_sOz_s-plane, especially when $\delta_{xz}^{(f)}$ is a monotonic function, the SD vectors will form a helical structure, otherwise they will create 'waves'.

Here we observe the SD vectors along oblique rays in the y_sOz_s-plane with θ_b denoting the oblique angle from the $+z_s$ axis to the ray. In Fig. 5, the oblique rays are shown, where the dashed black lines represent the rays with $\theta_b = \pm 5°$ and the dashed white lines are the rays with $\theta_b = \pm 3°$ (here $\alpha = 60°$). We can find that when the rays pass through the region between a pair of SD singularities, for instance the ray with $\theta_b = \pm 3°$, $\delta_{xz}^{(f)}$ decreases monotonically. This can be seen more directly in Fig. 6 where $\delta_{xz}^{(f)}$ is plotted as a function of z_s along the oblique rays. Fig. 6 shows that when $\theta_b = 3°$, the Gouy phase

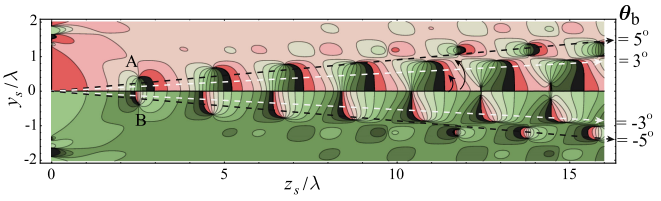

Fig. 5. Illustration of oblique rays in the y_sOz_s-plane. Here θ_b denotes the oblique angle between the oblique ray and the $+z_s$ axis.

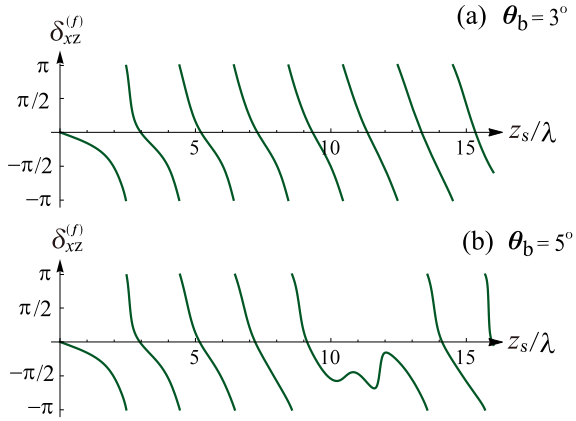

Fig. 6. Gouy phase difference $\delta_{xz}^{(f)}$ along oblique rays in the y_sOz_s-plane. (a)$\theta_b = 3°$, (b)$\theta_b = 5°$. Here $\alpha = 60°$.

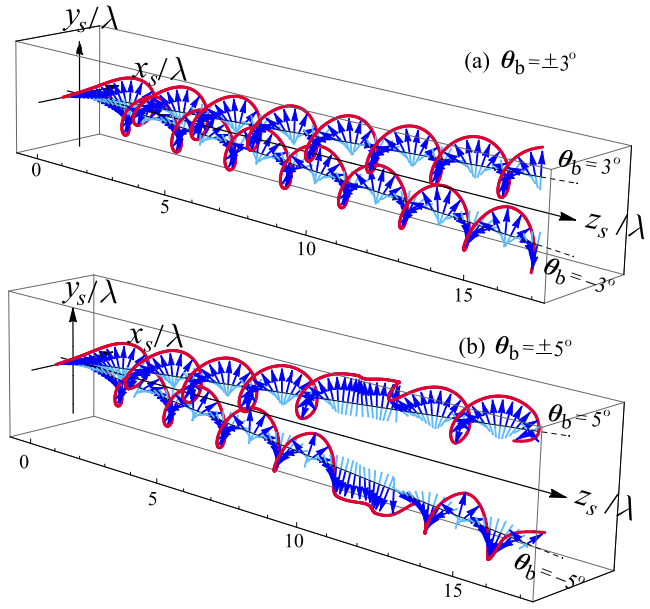

Fig. 7. SD vector twists along oblique rays in the y_sOz_s-plane. (a)$\theta_b = \pm 3°$, (b)$\theta_b = \pm 5°$. Here $\alpha = 60°$.

difference $\delta_{xz}^{(f)}$ is a monotonic function of z_s in the range of $0 < z_s < 16\lambda$, whereas the monotonic property of $\delta_{xz}^{(f)}$ does not hold in $10\lambda < z_s < 12\lambda$ as θ_b increases to 5°. Note that $\delta_{xz}^{(f)}$ is a periodic function, and the 'monotonic' here means that in its each period $\delta_{xz}^{(f)}$ decreases/increases monotonically.

The SD vectors along the oblique rays corresponding to the dashed lines in Fig. 5 are shown in Fig. 7, where the

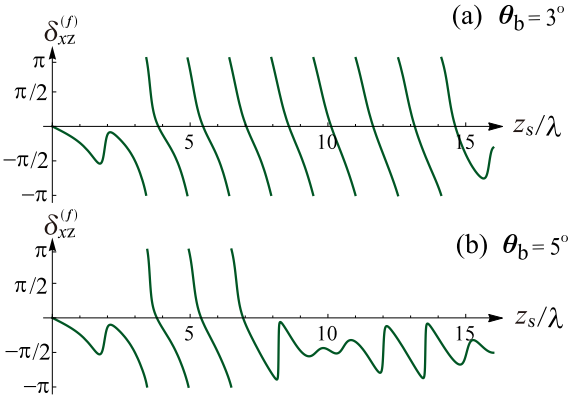

Fig. 8. Gouy phase difference $\delta_{xz}^{(f)}$ along oblique rays in the y_sOz_s-plane. (a)$\theta_b = 3°$, (b)$\theta_b = 5°$. Here $\alpha = 70°$.

blue arrows denote the SD vectors and the red curves around them indicate the envelope of the SD vectors. One can see that in the monotonic region, the SD vectors rotate clockwise along the propagation direction (see Fig. 7(a) for $\theta_b = \pm 3°$), while in the non-monotonic region, for instance in the range of $10\lambda < z_s < 12\lambda$ for $\theta_b = \pm 5°$ (Fig. 7(b)), the SD vectors 'wave' (i.e. move back and forth) there. Combined with analyses above, we can get that in the y_sOz_s-plane there can be multi-twists of SD vectors along a group of oblique rays (for instance the rays between points A and B in Fig. 5), namely the spiral twists in the monotonic region and the wave twists in the non-monotonic region. This implies that in the present focused field *the spiral structure of SD vectors* can exist in a wider region, a 2D space, rather than only along one fixed direction, i.e. the 1D propagation axis in previous studies [19]–[22], [25], [26]. Furthermore, the present 3D field is constructed without optical vortex, and this also indicates that *although the spiral structure of SD vectors can be a result of SOIs [19]–[21], [37], the OAM is not a necessary condition for this special structure (despite the fact that the OAM were used in all previous studies).*

Next, we show that these twists of SD vectors can vary with the strings of SD singularities. As it is discussed in sec. 3.1, if α changes, the topological reaction of the SD singularities can take place and the strings of SD singularities will move. When α increases to 70°, the curves of the Gouy phase difference $\delta_{xz}^{(f)}$ along the oblique rays $\theta_b = 3°, 5°$ are illustrated in Fig. 8, and the SD vectors along the oblique rays of $\theta_b = \pm 3°, \pm 5°$ are drawn in Fig. 9. First, by observing Fig. 8 and Fig. 4(b), we can see that since the annihilation of the SD singularities (points A and B), the range (about) $0 < z_s < 2\lambda$ becomes non-monotonic (see Fig. 8(a) and Fig. 8(b)), thus there the SD vectors exhibit the wave twists (see Fig. 9(a) and (b)). Second, because the positions of the SD strings move closer to the axis, the non-monotonic range for $\theta_b = 5°$ becomes wider. This can be seen in Fig. 8(b) where the non-monotonic range is $8\lambda < z_s < 16\lambda$. While for $\alpha = 60°$ the non-monotonic range is only $10\lambda < z_s < 12\lambda$ in Fig. 6(b). So, in Fig. 9(b) the 'wave' structure of the SD vectors is longer than that in Fig. 7(b). Third, the Gouy phase difference $\delta_{xz}^{(f)}$ along the ray with $\theta_b = 3°$ changes faster in $\alpha = 70°$ than it does in $\alpha = 60°$. In other words, the absolute value of the slope

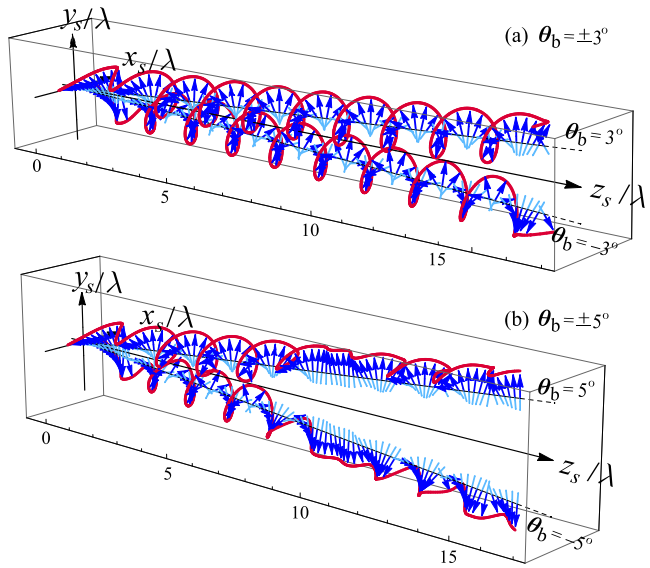

Fig. 9. SD vector twists along oblique rays in the y_sOz_s-plane. (a)$\theta_b = \pm 3°$, (b)$\theta_b = \pm 5°$. Here $\alpha = 70°$.

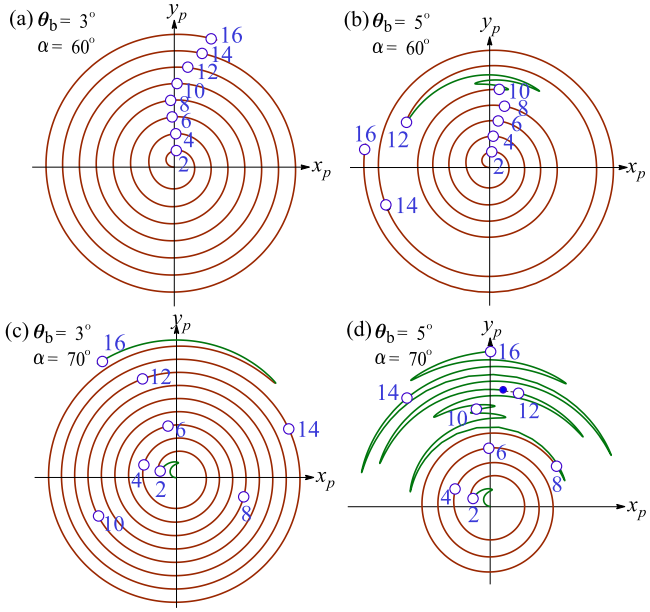

Fig. 10. The rotation behaviors expressed by the parametric plots. (a)$\theta_b = 3°$, $\alpha = 60°$; (b)$\theta_b = 5°$, $\alpha = 60°$; (c)$\theta_b = 3°$, $\alpha = 70°$; $\theta_b = 5°$, $\alpha = 70°$. The numbers 2, 4,... 16 represent the values of z_s (unit: λ).

of $\delta_{xz}^{(f)}$ for $\alpha = 70°$ is generally bigger than that for $\alpha = 60°$. This is caused by the emergence of more SD singularities when α increases from 60° to 70°. This is obvious in Fig. 9(a) that along each oblique ray the spiral twist has more circles (about 8 circles) than them in Fig. 7(a) (about 7 circles).

The rotation behavior of the SD vector twists can also be observed conveniently by a 2D parametric curve with z_s as the parameter. This is shown in Fig. 10, where $x_p = z_s * s_E^{(x)}$, $y_p = z_s * s_E^{(y)}$, i.e., the radius of the curve reflects the propagation distance and the azimuthal angle denotes the rotation angle with respect to the oblique ray (four plots in Fig. 10 correspond to the twists in Figs. 7 and 9). Note that the x_p and y_p are not

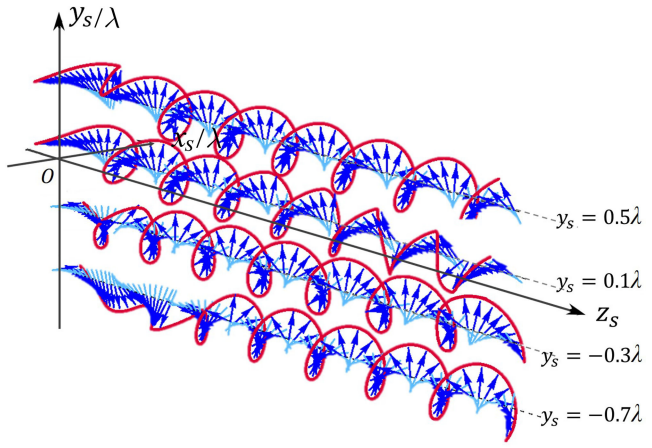

Fig. 11. SD vector twists along rays parallel with the z_s-axis in the y_sOz_s-plane. Here the plotting range is $0 < z_s < 16\lambda$, $\alpha = 60°$.

real physical quantities, thus their units are not shown. Here the curves are plotted from $z_s = 0$ to $z_s = 16\lambda$, and positions at $z_s = 2, 4, 6, \ldots, 16$ (unit: λ) are marked out by blue circles. The regions for the spiral twists are painted in red, while for the wave twists they are in green. It is obvious: when α increases from 60° to 70°, for the small oblique angle ($\theta_b = 3°$), the SD vectors rotate 'faster,' while for the big oblique angle ($\theta_b = 5°$), the spiral twisting region shrinks. Note in Fig. 10(d), there is a 'discontinuity' at point $z_s = 12\lambda$. This is caused by a SD singularity there.

In all above analyses, the twists of SD vectors are formed along oblique rays. Actually, this is not the only way to get the twisting structure of SD vectors in the y_sOz_s-plane. As we discussed previously, if the observation rays go through the region between two strings of SD singularities, the spiral structures of SD vectors can be constructed. So, at last, we show some other twists of SD vectors along different rays, see Fig. 11, where we still choose $\alpha = 60°$ and $0 < z_s \leq 16\lambda$. The observation rays there are not oblique but parallel with the z_s-axis. They are located at $y_s = 0.5\lambda, 0.1\lambda, -0.3\lambda, -0.7\lambda$. We can see firstly that the spiral structures are formed on all these four rays, and the SD vectors rotate clockwise along the propagation direction in the spiral region. Secondly, for the rays of $y_s = 0.5\lambda, -0.3\lambda$, the spiral twists occupy almost the whole range of the rays. This is because that the most ranges of these rays are located between String1 and String2 (see Fig. 3). Thirdly, the wave twists of SD vectors have relatively long ranges at the tail of the ray with $y_s = 0.1\lambda$ and at the head of the ray with $y_s = -0.7\lambda$. This is caused by the fact that in these ranges the rays are not between two strings of SD singularities.

In addition, all the results in this article are obtained and analyzed theoretically, while they also can be observed experimentally. The 3D vector field here can be generated by using a common high NA system [10], [20], [36], [39], [40], and the behaviors of SD vectors can be obtained through measuring total polarization states and the phases of the observed field via vectorial full-field reconstruction method [41] or by the nanoprobe scanning measurement [10], [20], [36].

IV. Conclusion

We propose a new and simple way to generate the spiral twists of SD vectors in a 3D focused field. In our method, the OAM is not used, which is different from and much easier than all reported methods. The spiral twists here can be formed in a wider space, a 2D space, instead of the 1D space in previous studies. The current method is based on constructing the spiral twists between the strings of SD singularities in a longitudinal plane, which is realized by focusing an HG10 beam with left-handed polarization in a high NA system. It is interesting to find that there the SD singularities can express themselves through a more direct physical quantity, the Gouy phase difference, which supplies us a convenient way to observe the SD singularities. The topological behaviors of the SD singularity strings and their effect on the twisting structures of SD vectors are also analyzed, and it is found that by increasing the semi-aperture angle α, the topological annihilation of the SD singularities will occur and the singularity strings will be closer to the central axis, so that the spiral structures of SD vectors will change into the wave structures in the annihilation region, while the spiral circles will increase along the rays closer to the axis.

The finding in this article suggests that the complicated singularities can manifest in an obvious way in optics. Our work will supply a new approach for controlling SD vectors in the 3D space, which may have applications in particle manipulation schemes, such as in the spin-dependent optical manipulation and in controlling light-matter interactions on the level of individual atoms [14], [20], [27], [28]. The present study may also be useful in applications for highly efficient spin-direction couplers [35]–[37].

References

[1] M. Born and E. Wolf, *Principles of Optics: Electromagnetic Theory of Propagation, Interference and Diffraction of Light, Seventh (expanded)* ed. Cambridge, U.K.: Cambridge University Press, 1999.

[2] E. Hecht, *Optics*, 5th ed. London, U.K.: Pearson Education, 2016.

[3] C. Shen, X. Bao, J. Tan, S. Liu, and Z. Liu, "Two noise-robust axial scanning multi-image phase retrieval algorithms based on pauta criterion and smoothness constraint," *Opt. Exp.*, vol. 25, no. 14, pp. 16 235–16 249, 2017.

[4] L. Allen, S. M. Barnett, and M. J. Padgett, *Optical Angular Momentum*. Bristol, U.K.: IoP Publishing, 2003.

[5] M. J. Padgett, J. Molloy, and D. McGloin, *Optical Tweezers: Methods and Applications*. Boca Raton, FL, USA: CRC Press, 2010.

[6] P. H. Jones, O. M. Maragò, and G. Volpe, *Optical Tweezers: Principles and Applications*. Cambridge, U.K.: Cambridge University Press, 2015.

[7] R. J. Patton and R. M. Reano, "Higher order mode conversion from Berry's phase in silicon optical waveguides," *IEEE Photon. J.*, vol. 13, no. 4, pp. 1–5, Aug. 2021.

[8] M. V. Berry and M. R. Dennis, "Polarization singularities in isotropic random vector waves," *Proc. R. Soc. A*, vol. 457, no. 2005, pp. 141–55, 2001.

[9] K. Y. Bliokh, A. Y. Bekshaev, and F. Nori, "Extraordinary momentum and spin in evanescent waves," *Nat. Commun.*, vol. 5, no. 3, 2014, Art. no. 3300.

[10] M. Neugebauer, T. Bauer, A. Aiello, and P. Banzer, "Measuring the transverse spin density of light," *Phys. Rev. Lett.*, vol. 114, no. 6, 2015, Art. no. 0 63901.

[11] S. Saha, A. K. Singh, S. K. Ray, A. Banerjee, S. D. Gupta, and N. Ghosh, "Transverse spin and transverse momentum in scattering of plane waves," *Opt. Lett.*, vol. 41, no. 19, pp. 4499–502, 2016.

[12] D. Sugic, M. R. Dennis, F. Nori, and K. Y. Bliokh, "Knotted polarizations and spin in three-dimensional polychromatic waves," *Phys. Rev. Res.*, vol. 2, 2020, Art. no. 0 42045.

[13] P. Banzer *et al.*, "The photonic wheel-demonstration of a state of light with purely transverse angular momentum," *J. Europ. Opt. Soc. Rap. Public.*, vol. 8, 2013, Art. no. 13032.

[14] A. Aiello, P. Banzer, M. Neugebauer, and G. Leuchs, "From transverse angular momentum to photonic wheels," *Nature Photon.*, vol. 9, no. 12, pp. 789–95, 2015.

[15] A. Y. Bekshaev, K. Y. Bliokh, and F. Nori, "Transverse spin and momentum in two-wave interference," *Phys. Rev. X*, vol. 5, no. 1, 2015, Art. no. 0 11039.

[16] W. Zhu, V. Shvedov, W. She, and W. Krolikowski, "Transverse spin angular momentum of tightly focused full poincaré beams," *Opt. Exp.*, vol. 23, no. 26, 2015, Art. no. 34029.

[17] A. Aiello and P. Banzer, "The ubiquitous photonic wheel," *J. Opt.*, vol. 18, no. 8, 2016, Art. no. 0 85605.

[18] J. Chen, C. Wan, L. Kong, and Q. Zhan, "Experimental generation of complex optical fields for diffraction limited optical focus with purely transverse spin angular momentum," *Opt. Exp.*, vol. 25, no. 8, pp. 8966–8974, Apr. 2017.

[19] X. Pang and W. Miao, "Spinning spin density vectors along the propagation direction," *Opt. Lett.*, vol. 43, no. 19, pp. 4831–34, 2018.

[20] J. S. Eismann, P. Banzer, and M. Neugebauer, "Spin-orbit coupling affecting the evolution of transverse spin," *Phys. Rev. Res.*, vol. 1, 2019, Art. no. 0 33143.

[21] F. Ye, J. Zou, and D. Deng, "The effect of the spin angular momentum on the tight-focusing vortex hollow Gaussian beams," *Ann. Phys.*, vol. 532, no. 4, 2020, Art. no. 1900548.

[22] X. Pang, W. Liu, and W. Miao, "Generation of spiral spin density vectors with a circularly polarized, vortex beam," *IEEE Photon. J.*, vol. 12, no. 2, Apr. 2020, Art. no. 6500514.

[23] Z. Man, X. Dou, and H. P. Urbach, "The evolutions of spin density and energy flux of strongly focused standard full poincaré beams," *Opt. Commun.*, vol. 458, 2020, Art. no. 124790.

[24] W. Miao, X. Pang, and W. Liu, "Photonic wheels and their topological reaction in a strongly focused amplitude tailored beam," *IEEE Photon. J.*, vol. 12, no. 2, Apr. 2020, Art. no. 6500709.

[25] J. Zhuang, L. Zhang, and D. Deng, "Tight-focusing properties of linearly polarized circular airy gaussian vortex beam," *Opt. Lett.*, vol. 45, no. 2, pp. 296–299, 2020.

[26] S. S. Stafeev and V. V. Kotlyar, "Invariance of the transverse spin angular momentum at the focus," *Opt. Commun.*, vol. 479, 2021, Art. no. 126453.

[27] C. Junge, D. O'shea, J. Volz, and A. Rauschenbeutel, "Strong coupling between single atoms and nontransversal photons," *Phys. Rev. Lett.*, vol. 110, no. 21, 2013, Art. no. 213604.

[28] M. Neugebauer, T. Bauer, P. Banzer, and G. Leuchs, "Polarization tailored light driven directional optical nanobeacon," *Nano Lett.*, vol. 14, no. 5, pp. 2546–2551, 2014.

[29] A. Aiello, N. Lindlein, C. Marquardt, and G. Leuchs, "Transverse angular momentum and geometric spin hall effect of light," *Phys. Rev. Lett.*, vol. 103, no. 10, 2009, Art. no. 100401.

[30] K. Y. Bliokh and F. Nori, "Relativistic hall effect," *Phys. Rev. Lett.*, vol. 108, Mar. 2012, Art. no. 120403.

[31] J. Korger *et al.*, "Observation of the geometric spin hall effect of light," *Phys. Rev. Lett.*, vol. 112, no. 11, 2014, Art. no. 113902.

[32] M. Neugebauer *et al.*, "Geometric spin hall effect of light in tightly focused polarization-tailored light beams," *Phys. Rev. A*, vol. 89, no. 1, 2014, Art. no. 0 13840.

[33] K. Y. Bliokh, D. Smirnova, and F. Nori, "Quantum spin hall effect of light," *Science*, vol. 348, no. 6242, pp. 1448–1451, 2015.

[34] X. Ling *et al.*, "Recent advances in the spin hall effect of light," *Rep. Prog. Phys.*, vol. 80, no. 6, 2017, Art. no. 0 66401.

[35] K. Y. Bliokh and F. Nori, "Transverse and longitudinal angular momenta of light," *Phys. Rep.*, vol. 592, pp. 1–38, 2015.

[36] J. S. Eismann *et al.*, "Transverse spinning of unpolarized light," *Nat. Photon.*, vol. 15, no. 2, pp. 156–161, 2021.

[37] K. Y. Bliokh, F. J. Rodríguez-Fortuño, F. Nori, and A. V. Zayats, "Spin-orbit interactions of light," *Nat. Photon.*, vol. 9, no. 12, pp. 156–163, 2015.

[38] I. Freund, "Cones, spirals, and möbius strips, in elliptically polarized light," *Opt. Commun.*, vol. 249, no. 1-3, pp. 7–22, 2005.

[39] T. Bauer *et al.*, "Observation of optical polarization möbius strips," *Science*, vol. 347, no. 6225, pp. 964–966, 2015.

[40] T. Bauer, M. Neugebauer, G. Leuchs, and P. Banzer, "Optical polarization möbius strips and points of purely transverse spin density," *Phys. Rev. Lett.*, vol. 117, no. 1, 2016, Art. no. 0 13601.

[41] D. Sugic *et al.*, "Particle-like topologies in light," *Nat. Commun.*, vol. 12, no. 1, pp. 1–10, 2021.

[42] M. R. Dennis, R. P. King, B. Jack, K. O'Holleran, and M. J. Padgett, "Isolated optical vortex knots," *Nat. Phys.*, vol. 6, no. 2, pp. 118–21, 2010.
[43] H. Larocque *et al.*, "Reconstructing the topology of optical polarization knots," *Nat. Phys.*, vol. 14, no. 11, pp. 1079–82, 2018.
[44] I. Freund and N. Shvartsman, "Wave-field phase singularities: The sign principle," *Phys. Rev. A*, vol. 50, no. 6, pp. 5164–72, 1994.
[45] I. Freund and D. A. Kessler, "Critical point trajectory bundles in singular wave fields," *Opt. Commun.*, vol. 187, no. 1-3, pp. 71–90, 2001.
[46] M. V. Berry, "Circular lines of circular polarization in three dimensions, and their transverse-field counterparts," *J. Opt.*, vol. 15, no. 4, 2013, Art. no. 0 44024.
[47] I. Freund, "Observer-dependent sign inversions of polarization singularities," *Opt. Lett.*, vol. 39, no. 20, pp. 5873–76, 2014.
[48] X. Pang, C. Feng, B. Nyamdorj, and X. Zhao, "Hidden singularities in 3 d vector fields," *J. Opt.*, vol. 22, no. 11, 2020, Art. no. 115605.
[49] X. Pang, T. D. Visser, and E. Wolf, "Phase anomaly and phase singularities of the field in the focal region of high-numerical aperture systems," *Opt. Commun.*, vol. 284, pp. 5517–5522, 2011.
[50] K. Y. Bliokh, P. Schattschneider, J. Verbeeck, and F. Nori, "Electron vortex beams in a magnetic field: A new twist on landau levels and aharonov-bohm states," *Phys. Rev. X*, vol. 2, 2012, Art. no. 0 41011.
[51] G. Guzzinati, P. Schattschneider, K. Y. Bliokh, F. Nori, and J. Verbeeck, "Observation of the larmor and gouy rotations with electron vortex beams," *Phys. Rev. Lett.*, vol. 110, 2013, Art. no. 0 93601.
[52] J. T. Verdeyen, *Laser Electronics*, 3rd ed. Hoboken, NJ, USA: Prentice Hall, 1994.
[53] B. Richards and E. Wolf, "Electromagnetic diffraction in optical systems, II. structure of the image field in aplanatic systems," *Proc. R. Soc. A*, vol. 253, pp. 358–379, 1959.